JACS
JOURNAL OF THE AMERICAN CHEMICAL SOCIETY
Article
pubs.acs.org/JACS

Thermochemical Insight into the Reduction of CO to CH_3OH with $[Re(CO)]^+$ and $[Mn(CO)]^+$ Complexes

Eric S. Wiedner* and Aaron M. Appel

Physical Sciences Division, Pacific Northwest National Laboratory, P.O. Box 999, K2-57, Richland, Washington 99352, United States

Supporting Information

ABSTRACT: To gain insight into thermodynamic barriers for reduction of CO into CH_3OH, free energies for reduction of $[CpRe(PPh_3)(NO)(CO)]^+$ into $CpRe(PPh_3)(NO)(CH_2OH)$ have been determined from experimental measurements. Using model complexes, the free energies for the transfer of H^+, H^-, and e^- have been determined. A pK_a of 10.6 was estimated for $[CpRe(PPh_3)(NO)(CHOH)]^+$ by measuring the pK_a for the analogous $[CpRe(PPh_3)(NO)(CMeOH)]^+$. The hydride donor ability ($\Delta G^\circ_{H^-}$) of $CpRe(PPh_3)(NO)(CH_2OH)$ was estimated to be 58.0 kcal mol^{-1}, based on calorimetry measurements of the hydride-transfer reaction between $CpRe(PPh_3)(NO)(CHO)$ and $[CpRe(PPh_3)(NO)(CHOMe)]^+$ to generate the methylated analogue, $CpRe(PPh_3)(NO)(CH_2OMe)$. Cyclic voltammograms recorded on $CpRe(PPh_3)(NO)(CMeO)$, $CpRe(PPh_3)(NO)(CH_2OMe)$, and $[CpRe(PPh_3)(NO)(CHOMe)]^+$ displayed either a quasireversible oxidation (neutral species) or reduction (cationic species). These potentials were used as estimates for the oxidation of $CpRe(PPh_3)(NO)(CHO)$ or $CpRe(PPh_3)(NO)(CH_2OH)$ or the reduction of $[CpRe(PPh_3)(NO)(CHOH)]^+$. Combination of the thermodynamic data permits construction of three-dimensional free energy landscapes under varying conditions of pH and P_{H_2}. The free energy for H_2 addition ($\Delta G^\circ_{H_2}$) to $[CpRe(PPh_3)(NO)(CO)]^+$ (+15 kcal mol^{-1}) was identified as the most significant thermodynamic impediment for the reduction of CO. DFT computations on a series of $[Cp^XM(L)(NO)(CO)]^+$ (M = Re, Mn) complexes indicate that $\Delta G^\circ_{H_2}$ can be varied by 11 kcal mol^{-1} through variation of both the ancillary ligands and the metal.

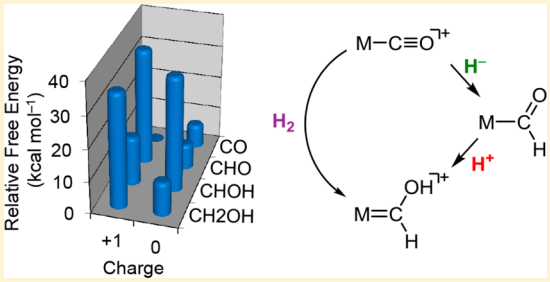

INTRODUCTION

The multiproton and multielectron reduction of CO_2 has been studied widely as a route for production of liquid fuels from renewable energy sources such as sunlight.[1−7] Many molecular electrocatalysts for reduction of CO_2 produce either CO or formic acid in a $2e^-/2H^+$ process instead of more reduced products such as methanol.[7−9] Industrial technologies currently exist for the conversion of syngas (CO/H_2) into methanol, liquid hydrocarbons, or methane.[10−12] However, industrial syngas conversion is performed at elevated temperatures and pressures on a large scale at centralized facilities, which may not be economically viable for energy storage from disperse renewable energy sources such as solar energy.[7,13,14] In contrast, a tandem electrocatalytic system composed of separate electrocatalysts for reduction of CO_2 and CO could lead to decentralized production of renewable methanol or other liquid fuels.[9] Therefore, developing an understanding of how to design electrocatalysts for the reduction of CO will be of interest.

Many mechanistic studies have been conducted on the reduction of homogeneous transition-metal carbonyl complexes as models for catalytic processes.[15−19] A reduction pathway that is frequently considered in homogeneous systems is the sequential transfer of hydride (H^-) and proton (H^+) equivalents to a coordinated CO ligand to afford formyl (CHO, step 1), hydroxycarbene (CHOH, step 2), and hydroxymethyl (CH_2OH, step 3) intermediates, as illustrated in Scheme 1.[20,21] Hydroxymethyl complexes have been shown to react with further H^+/H^- equivalents to produce CH_3OH (step 4) or CH_4[22,23] or to form new C−C bonds via CO insertion.[24−26] This reduction sequence could also be envisioned as an electrochemical cycle in which the H^- equivalents are generated in a $2e^-/1H^+$ process at a second

Scheme 1. Proposed Cycle for Production of CH_3OH from $[M(CO)]^+$

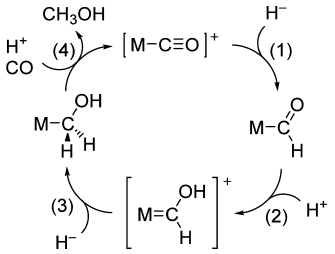

Received: March 6, 2014
Published: May 22, 2014

   dx.doi.org/10.1021/ja502316e | J. Am. Chem. Soc. 2014, 136, 8661−8668

metal center such as $[M(diphosphine)_2]^{2+}$ (M = Ni, Pd, Pt).[27] Previous studies have demonstrated intermolecular H^- transfer from $[HM(diphosphine)_2]^+$ (M = Ni, Pt) species to transition-metal carbonyl complexes,[27−30] thus providing a foundation for an electrocatalytic CO reduction cycle.

Successful development of an electrocatalytic process for CO reduction will be facilitated by a system in which the free energy requirements of each step are carefully balanced. Thermodynamic information on reduction of $[M(CO)]^+$ complexes has been reported for several metal platforms. Wayland has measured equilibrium constants for insertion of CO into Rh−H bonds to afford [Rh(porphyrin)(CHO)] complexes.[31−35] DuBois measured hydride donor abilities ($\Delta G^\circ_{H^-}$) and C−H bond dissociation free energies (BDFE) for a series of $Cp^XRe(L)(NO)(CHO)$ complexes.[28,36] More recently, Bercaw reported $\Delta G^\circ_{H^-}$ and pK_a values for several $[Re(PBH)(CO)_4(CHO)]^+$ complexes, where PBH is a phosphine ligand containing a protonated pendant base.[30] However, these studies have focused on the initial reduction step to generate the formyl ligand and not the subsequent steps required for further reduction of the formyl ligand with H^+/H^- equivalents.

Significant challenges exist for performing experimental measurements on the thermodynamics of $[M(CO)]^+$ reduction. One challenge is that many M(CHO) and $M(CH_2OH)$ species are thermally unstable at ambient temperature,[17,26] thus limiting the range of complexes for which useful measurements can be made. A second challenge is that M(CHO) and $M(CH_2OH)$ complexes react irreversibly with protons (or other Lewis acids) to afford $M(CH_3)$ complexes due to intermolecular H^- transfer and C−O bond cleavage.[20,21,37]

Herein we report thermodynamic measurements for reduction of $[CpRe(PPh_3)(NO)(CO)]^+$ to $CpRe(PPh_3)(NO)(CH_2OH)$, completing the previous thermodynamic measurements of this system[28] to include steps for reduction past $CpRe(PPh_3)(NO)(CHO)$. Key to this study is the use of model complexes that do not undergo C−H and C−O bond cleavage reactions that preclude measurement of the desired thermodynamic properties. The thermochemical data allow us to construct free-energy landscapes for reduction of $[CpRe(PPh_3)(NO)(CO)]^+$ and identify high-energy intermediates that hinder development of an electrocatalytic system for reduction of CO. Finally, DFT computations on a series of $[Cp^XM(L)(NO)(CO)]^+$ (M = Re, Mn) complexes are utilized to investigate the effects of structural modification on improving the energy matching of intermediates to facilitate CO reduction.

RESULTS

pK_a Measurement. The pK_a of $[CpRe(PPh_3)(NO)(CHOH)]^+$ (eq 1, R = H) is the thermodynamic half-reaction

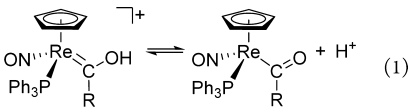

(1)

that corresponds to step 2 of the $[M(CO)]^+$ reduction cycle in Scheme 1. Hydride transfer from $CpRe(PPh_3)(NO)(CHO)$ to $[CpRe(PPh_3)(NO)(CHOH)]^+$ is known to be rapid and irreversible,[20] which prevents direct measurement of this pK_a value due to decomposition into $[CpRe(PPh_3)(NO)(CO)]^+$ and $CpRe(PPh_3)(NO)(CH_3)$. In contrast, the closely related acetyl complex, $CpRe(PPh_3)(NO)(CMeO)$,[38] is not capable of H^- transfer. Therefore, the pK_a of $[CpRe(PPh_3)(NO)(CMeOH)]^+$ in CD_3CN (eq 1, R = Me) was determined against *o*-toluidine (pK_a = 10.50 for the conjugate acid)[39] in both the forward and reverse reactions. The ^1H NMR spectrum of these reactions displayed an averaged set of resonances for $CpRe(PPh_3)(NO)(CMeO)$ and $[CpRe(PPh_3)(NO)(CMeOH)]^+$ due to fast chemical exchange, and an averaged set of resonances was also observed for *o*-toluidine and *o*-toluidinium (Figure S1). The ratios of all species were determined from the weighted averages of the chemical shifts, and an equilibrium constant of 0.8 ± 0.3 was determined for the reaction. This equilibrium constant, along with the pK_a of *o*-toluidinium in acetonitrile, can be used to calculate a pK_a of 10.6 ± 0.4 for $[CpRe(PPh_3)(NO)(CMeOH)]^+$.

Measurements of the Hydride Donor Ability. The hydride donor ability of $CpRe(PPh_3)(NO)(CH_2OH)$ (eq 2, R

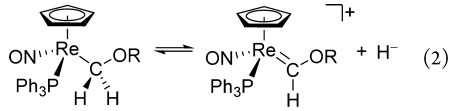

(2)

= H) is the thermodynamic half-reaction that corresponds to step 3 of the $[M(CO)]^+$ reduction cycle in Scheme 1. A previous report by Gladysz et al. indicated that the hydroxymethyl complex $CpRe(PPh_3)(NO)(CH_2OH)$ was not isolable, unlike the analogous methylated complex $CpRe(PPh_3)(NO)(CH_2OMe)$.[20] In an attempt to measure an equilibrium hydride transfer, a solution of $CpRe(PPh_3)(NO)(CH_2OMe)$ in CD_3CN was treated with $[Cp^*Re(NO)(CO)_2]^+$ ($Cp^* = C_5Me_5$), which has a hydride acceptor ability ($-\Delta G^\circ_{H^-}$) of −52.6 kcal mol^{-1}.[28] However, this reaction was observed by ^1H NMR spectroscopy to produce equal amounts of the known complexes $[CpRe(PPh_3)(NO)(CHOMe)]^+$, $CpRe(PPh_3)(NO)(CH_3)$, and $Cp^*Re(NO)(CO)(COOMe)$ (Scheme S1 and Figures S2−S3).[20,40] These reaction products are consistent with transfer of MeO^- from $CpRe(PPh_3)(NO)(CH_2OMe)$ to $[Cp^*Re(NO)(CO)_2]^+$, followed by a rapid and irreversible H^- transfer from $CpRe(PPh_3)(NO)(CH_2OMe)$ to transient $[CpRe(PPh_3)(NO)(CH_2)]^+$.[20] No resonances could be observed for $Cp^*Re(NO)(CO)(CHO)$, which would be the product of H^- transfer from $CpRe(PPh_3)(NO)(CH_2OMe)$ to $[Cp^*Re(NO)(CO)_2]^+$. These results suggested that it is not feasible to obtain $\Delta G^\circ_{H^-}$ for $CpRe(PPh_3)(NO)(CH_2OMe)$ by measuring an equilibrium H^- transfer to an acceptor due to preferential MeO^- loss.

Hydride transfer from $CpRe(PPh_3)(NO)(CHO)$ to $[CpRe(PPh_3)(NO)(CHOMe)]^+$ (eq 3) was previously reported to be

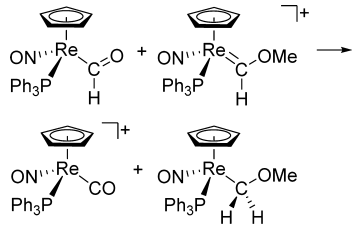

(3)

rapid and quantitative at −70 °C in CD_2Cl_2 solution,[20] and we found the same to be true when the reaction was performed in CD_3CN at 25 °C. Therefore calorimetric studies were performed to measure the enthalpy of this reaction. Using an isothermal titration calorimeter, 16 aliquots of an acetonitrile

dx.doi.org/10.1021/ja502316e | J. Am. Chem. Soc. 2014, 136, 8661−8668

solution of $[CpRe(PPh_3)(NO)(CHOMe)]^+$ were injected into an acetonitrile solution of $CpRe(PPh_3)(NO)(CHO)$ such that <10% of the formyl complex was consumed at the end of the titration. A reaction enthalpy (ΔH°_{rxn}) of −11.5 ± 2.6 kcal mol^{-1} was determined from six independent measurements. The size and charge of the reactants and products of eq 3 are similar, so ΔS°_{rxn} is expected to be negligible, and therefore ΔH°_{rxn} is expected to be approximately equal to ΔG°_{rxn}, within the experimental error. On this basis, $\Delta G^\circ_{H^-}$ of $CpRe(PPh_3)(NO)(CH_2OMe)$ was calculated to be 58.0 kcal mol^{-1} by using ΔG°_{rxn} for eq 3 (−11.5 kcal mol^{-1}) and the previously determined $\Delta G^\circ_{H^-}$ of $CpRe(PPh_3)(NO)(CHO)$ (46.5 kcal mol^{-1}).[28]

As a control experiment to cross-check the accuracy of the above calorimetric measurement, a reaction enthalpy of −7.0 kcal mol^{-1} was measured by calorimetry for H^- transfer from $CpRe(PPh_3)(NO)(CHO)$ to $[CpRe(NO)(CO)_2]^+$, shown in eq 4. The entropy change of this reaction is expected to be

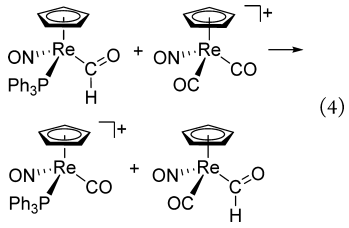

(4)

larger than that for eq 3, since the size and charge of the reactants and products in eq 4 are dissimilar. Hydride-transfer reactions have been proposed to be similar to electron-transfer reactions,[36] so the entropy change associated with eq 4 can be estimated using a semiempirical equation developed by Weaver for electron-transfer reactions.[41] By using estimated radii of 3.0 and 4.5 Å for $[CpRe(NO)(CO)_2]^+$ and $[CpRe(PPh_3)(NO)(CO)]^+$, an entropy change of +2.3 cal mol^{-1} K^{-1} can be calculated for eq 4, which contributes −0.7 kcal mol^{-1} to the reaction free energy. The combined ΔH°_{rxn} and ΔS°_{rxn} values afford ΔG°_{rxn} = −7.7 kcal mol^{-1} for eq 4, which is in good agreement with the free energy change of −8.5 kcal mol^{-1} calculated from the experimentally measured $\Delta G^\circ_{H^-}$ values of $CpRe(PPh_3)(NO)(CHO)$ and $CpRe(NO)(CO)(CHO)$.[28]

Electrochemistry. A cyclic voltammogram showing oxidation of $CpRe(PPh_3)(NO)(CMeO)$ in acetonitrile solution at a scan rate (υ) of 10 V s^{-1} is presented in Figure 1a and is consistent with a one-electron oxidation from Re(I) to a chemically unstable Re(II) species. Partial chemical reversibility is observed for this oxidation as measured by the i_{pc}/i_{pa} value of 0.26, where i_{pc}/i_{pa} is the ratio of the cathodic peak current (i_{pc}) to the anodic peak current (i_{pa}). An $E_{1/2}$ value of +0.20 V vs $Cp_2Fe^{+/0}$ (the reference couple for all potentials in this paper) was measured for the oxidation of $CpRe(PPh_3)(NO)(CMeO)$ at υ = 10 V s^{-1} with a peak-to-peak separation (ΔE_p) of 100 mV. The irreversible chemical reaction is not expected to affect the measured peak potentials under conditions in which i_{pc}/i_{pa} can be measured,[42,43] thus the measured $E_{1/2}$ is expected to be a reasonable estimate for E° of the Re(II/I) couple. A similar oxidation wave was observed for $CpRe(PPh_3)(NO)(CH_2OMe)$ (Figure 1b) with i_{pc}/i_{pa} = 0.51 and $E_{1/2}$ = +0.03 V (ΔE_p = 84 mV) at υ = 10 V s^{-1}. We assign an error of ±0.03 V to these $E_{1/2}$ values, which reflects variability in the measured peak potentials and possible differences in resistance losses (iR drop) at higher scan rates for a wave with i_{pc}/i_{pa} < 1. The oxidation wave for $CpRe(PPh_3)(NO)(CHO)$ was completely irreversible

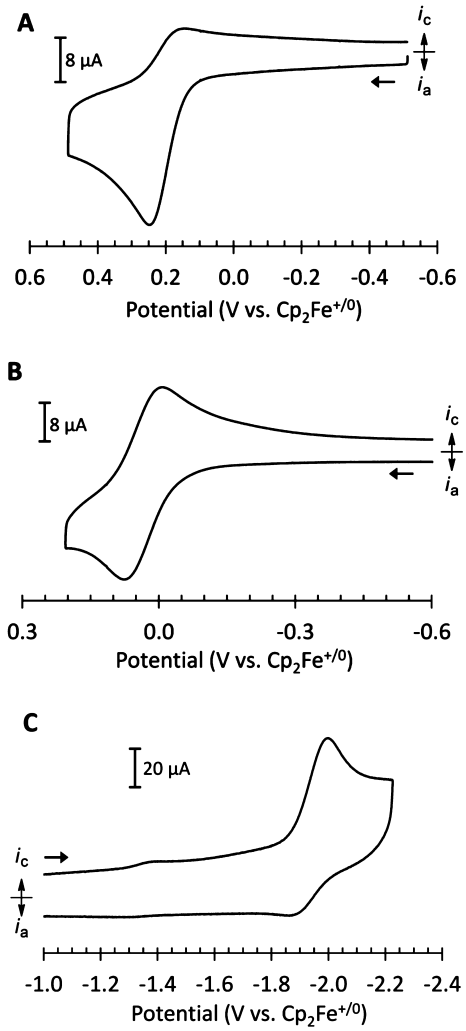

Figure 1. Cyclic voltammograms showing the Re(II/I) couple of $CpRe(PPh_3)(NO)(CMeO)$ (A) and $CpRe(PPh_3)(NO)(CH_2OMe)$ (B), and the Re(I/0) couple of $[CpRe(PPh_3)(NO)(CHOMe)]^+$ (C). Conditions: 1 mM analyte, 0.2 M NBu_4PF_6 in MeCN solution, υ = 10 V s^{-1}(A,B) or 50 V s^{-1} (C), 1 mm diameter glassy carbon electrode.

at υ = 10 V s^{-1} (Figure S4), though the measured peak potential of +0.17 V is similar to the $E_{1/2}$ of +0.20 V that was measured for $CpRe(PPh_3)(NO)(CMeO)$.

A quasireversible reduction wave with $i_{pa}/i_{pc} \approx 0.20$ was observed at $E_{1/2}$ = −1.93 V (ΔE_p = 144 mV) in cyclic voltammograms of $[CpRe(PPh_3)(NO)(CHOMe)]^+$ recorded at υ = 50 V s^{-1} (Figure 1c). This reduction wave is assigned to the Re(I/0) couple for simplicity, though it is likely that the unpaired electron of the reduced product is delocalized onto the NO ligand. The Re(I/0) couple of $[CpRe(PPh_3)(NO)(CHOMe)]^+$ is 590 mV more negative than the Re(I/0) of $[CpRe(PPh_3)(NO)(CO)]^+$ ($E_{1/2}$ = −1.34 V),[28] consistent with the CO ligand being more electron withdrawing than the CHOMe ligand. A reduction wave was observed for $[CpRe(PPh_3)(NO)(CHOH)]^+$ at a similar potential but was completely irreversible, even at scan rates of 50 V s^{-1} (Figure S5).

Thermochemical Cycles. By utilizing established thermodynamic cycles,[44−50] the experimental measurements described above can be used to construct the thermochemical diagram in Scheme 2. This diagram illustrates the energetics in acetonitrile solution of the CHO, CHOH, and CH_2OH ligands in terms of

dx.doi.org/10.1021/ja502316e | J. Am. Chem. Soc. 2014, 136, 8661−8668

Scheme 2. Experimental Thermochemical Data for $[CpRe(PPh_3)(NO)(CO)]^+$ and Related Species in Acetonitrile Solution, Showing the Relationships Between $E_{1/2}$, pK_a, BDFE, $\Delta G^\circ_{H^-}$, and $\Delta G^\circ_{H_2}$ Values[a]

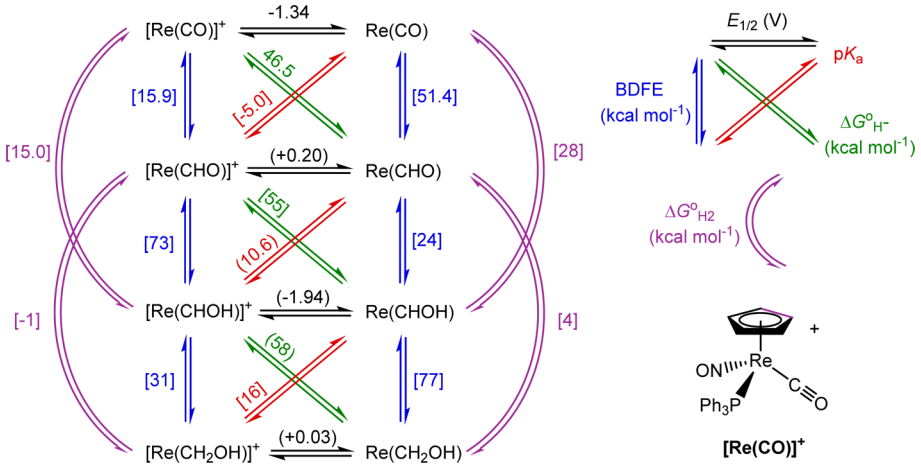

[a]Values in parentheses were estimated from experimental measurements of model complexes, and values in brackets were determined using the measured values and thermodynamic cycles.

their Brønsted–Lowry acidities (pK_a), homolytic bond dissociation free energies (BDFE), and hydride donor abilities ($\Delta G^\circ_{H^-}$). In construction of the diagram, the pK_a, $\Delta G^\circ_{H^-}$, and $E_{1/2}$ values measured for the model, methyl substituted complexes are assumed to be equivalent to the values of the Re(CHO), $[Re(CHOH)]^+$, and $Re(CH_2OH)$ complexes, and the values of the surrogates are listed in parentheses in Scheme 2. When only two sides of a triangle within this scheme were known, the third side was calculated by completion of a thermochemical cycle to give the values that were not directly measured, which are listed in brackets in Scheme 2. Each thermochemical cycle used to complete this diagram is tabulated in the Supporting Information with estimates of experimental uncertainty.

In Scheme 2, $[CpRe(PPh_3)(NO)(CHOH)]^+$ can be described as resulting from addition of H_2 to the CO ligand of $[CpRe(PPh_3)(NO)(CO)]^+$. The free energy of H_2 addition ($\Delta G^\circ_{H_2}$) to $[CpRe(PPh_3)(NO)(CO)]^+$, denoted by a purple arrow in Scheme 2, was calculated to be +15.0 ± 0.7 kcal mol^{-1} using a thermochemical cycle composed of $\Delta G^\circ_{H^-}$ of $CpRe(PPh_3)(NO)(CHO)$, the pK_a of $[CpRe(PPh_3)(NO)(CHOH)]^+$, and the free energy for heterolytic cleavage of H_2 (Scheme 3). Values of $\Delta G^\circ_{H_2}$ were also calculated for

Scheme 3. Thermochemical Cycle for Determination of the Free Energy of H_2 Addition ($\Delta G^\circ_{H_2}$) to $[CpRe(PPh_3)(NO)(CO)]^+$

$[Re(CO)]^+ + H^- \rightarrow Re(CHO)$	$-\Delta G^\circ_{H-}$
$Re(CHO) + H^+ \rightarrow [Re(CHOH)]^+$	$-1.364 \times pK_a$
$H_2 \rightarrow H^+ + H^-$	76.0 kcal mol^{-1}
$[Re(CO)]^+ + H_2 \rightarrow [Re(CHOH)]^+$	ΔG°_{H2}

$CpRe(PPh_3)(NO)(CO)$ (+28 ± 3 kcal mol^{-1}), $CpRe(PPh_3)(NO)(CHO)$ (+4 ± 4 kcal mol^{-1}), and $[CpRe(PPh_3)(NO)(CHO)]^+$ (−1 ± 6 kcal mol^{-1}) using thermochemical cycles similar to the one in Scheme 3. These results indicate that reduction of the CO ligand by H_2 is significantly more challenging than reduction of the CHO ligand.

Density functional theory (DFT) was employed to determine the effect of changing the ancillary ligands or the identity of the metal on the thermodynamics for reduction of the CO ligand. Using an isodesmic protocol that has been demonstrated to have a mean absolute error of 1.4 kcal mol^{-1} for computation of M–H bond strengths,[51] a series of isodesmic reactions were constructed in which H_2 is transferred from $[Cp^XM(L)(NO)(CHOH)]^+$ (M = Re, Mn) to a reference species, $[CpRe(PPh_3)(NO)(CO)]^+$, as shown in eq 5. The values of $\Delta G^\circ_{H_2}$ for the $[Cp^XM(L)(NO)(CHOH)]^+$ complexes were then determined from the computed free energy for eq 5 and the experimentally determined $\Delta G^\circ_{H_2}$ value of $[CpRe(PPh_3)(NO)(CO)]^+$. Values of $\Delta G^\circ_{H^-}$ have been reported for the analogous series of $Cp^XRe(L)(NO)(CHO)$ complexes[28,36] but not for $Cp^XMn(L)(NO)(CHO)$. Therefore, a second isodesmic reaction was utilized to compute values of $\Delta G^\circ_{H^-}$ for $Cp^XMn(L)(NO)(CHO)$ relative to $CpRe(PMe_3)(NO)(CHO)$ (eq 6). The resulting values of these computations are provided in Table 1, along with pK_a values of $[Cp^XM(L)(NO)$-

Table 1. Thermodynamic Properties for $[Cp^XM(L)(NO)(CO)]^+$ and Related Species in Acetonitrile Solution

	$\Delta G^\circ_{H_2}$ of $[M(CO)]^+$[b]		$\Delta G^\circ_{H^-}$ of M(CHO)[c]		pK_a of $[M(CHOH)]^+$[d]	
Cp^X/L[a]	Re	Mn	Re	Mn	Re	Mn
Cp/CO	17.5	13.2	55.0	56.7	2.6	4.5
Cp*/CO	16.2	10.4	52.6	51.6	5.3	10.3
Cp/PPh_3	15.0[e]	8.9	46.5	44.7	10.6	16.4
Cp/PMe_3	15.4	8.8	44.1	42.3	12.1	18.3
Cp*/PMe_3	13.2	6.7	42.1	39.6	15.2	21.8

[a]Cp* = C_5Me_5. [b]Computed by DFT using eq 5 and listed in units of kcal mol^{-1}. [c]Experimental values of Re from refs 28 and 36, Mn values computed by DFT using eq 6, in units of kcal mol^{-1}. [d]Determined from a thermochemical cycle using $\Delta G^\circ_{H_2}$ and $\Delta G^\circ_{H^-}$ (see Scheme 3). [e]This value was measured experimentally and was used as the reference for the DFT isodesmic reactions (and therefore matches experiment by construction).

dx.doi.org/10.1021/ja502316e | J. Am. Chem. Soc. 2014, 136, 8661–8668

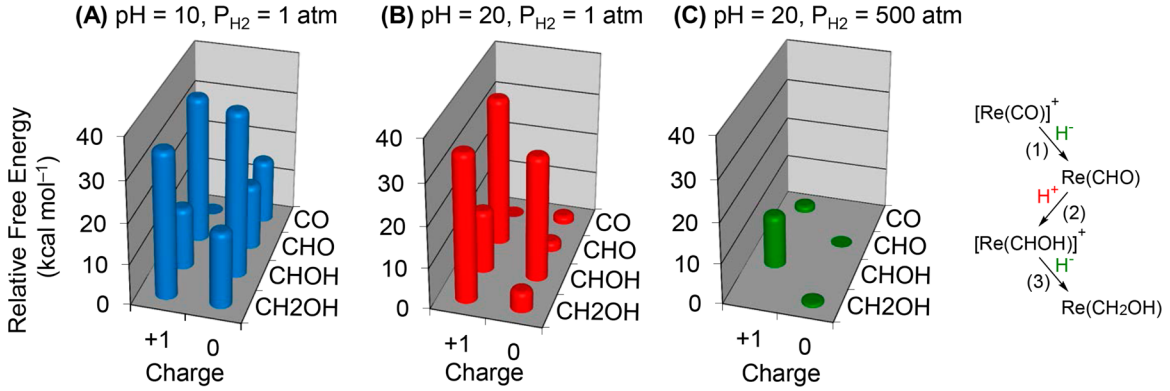

Figure 2. Free energy landscapes in acetonitrile, showing the relative free energies of $[Re(CO)]^{+/0}$, $[Re(CHO)]^{+/0}$, $[Re(CHOH)]^{+/0}$, and $[Re(CH_2OH)]^{+/0}$ species under varying conditions of pH and P_{H_2}. Right: Reduction of $[Re(CO)]^+$ to $Re(CH_2OH)$ via a $H^-/H^+/H^-$ pathway.

$(CHOH)]^+$ calculated from the thermodynamic relationships in Scheme 3.

$$[M(CHOH)]^+ + [Re(CO)]^+_{ref} \rightarrow [M(CO)]^+ + [Re(CHOH)]^+_{ref} \quad (5)$$

$$Mn(CHO) + [Re(CO)]^+_{ref} \rightarrow [Mn(CO)]^+ + Re(CHO)_{ref} \quad (6)$$

DISCUSSION

Free Energy Landscapes for Reduction of a CO Ligand. The thermochemical diagram in Scheme 2 contains valuable information for prediction of chemical reactivity. However, reaction pathways under non-standard state conditions can be difficult to envision from Scheme 2, in which the energetics of individual reaction steps are depicted in a numerical format under standard state conditions (pH = 0 and P_{H_2} = 1 atm). Presentation of the thermochemical information in a three-dimensional free energy landscape (also called a free energy map) permits more facile visualization of possible reaction pathways under varying conditions of pH and P_{H_2}.[47]

To construct a free energy landscape, the relative free energy for each species is determined under a specified set of conditions (e.g., pH = 10 and P_{H_2} = 1 atm in acetonitrile). The layout for the base is similar to Scheme 2, where the charge decreases from left to right and the number of C−H and O−H bonds increases from back to front. The vertical height of each bar corresponds to the free energy of the species relative to the most stable species under the specified conditions. For example, $[Re(CO)]^+$ is the most stable species at pH = 10 and P_{H_2} = 1 atm in acetonitrile, and its free energy is set to 0 kcal mol^{-1} under these conditions (Figure 2a). Each species differs from the adjacent species by transfer of a H^+, $H^•$, H^-, or e^- either to or from H^+ or H_2 in solution. Therefore, the free energies for interconversion between adjacent species are affected by either the solution pH (H^+ transfers) or P_{H_2} ($H^•$ transfers) or by both the solution pH and P_{H_2} (H^- and e^- transfers).[47] An interactive worksheet for generating free energy landscapes for reduction of $[CpRe(PPh_3)(NO)(CO)]^+$ is included as Supporting Information.

The utility of the free energy landscapes becomes evident when considering pathways by which $[Re(CO)]^+$ might be reduced to $Re(CH_2OH)$, as the energetically accessible species can be identified visually. Pathways involving reduction by either $H^•$ or e^- lead to the radical species $[Re(CHO)]^+$, Re(CHOH), or $[Re(CH_2OH)]^+$, which are all high-energy intermediates (>30 kcal mol^{-1}); thus reaction steps that produce radical intermediates are not likely to be viable for a catalytic system based upon these complexes. A sequential $H^-/H^+/H^-$ transfer pathway (Figure 2, right-hand side) also leads to one or more high-energy intermediates, though these intermediates are still lower in energy than the radical species produced by $H^•$ or e^- transfer. At P_{H_2} = 1 atm, the most difficult step of a $H^-/H^+/H^-$ pathway depends on the solution pH. For example, formation of Re(CHO) (step 1) is the most challenging step at low pH (+15.9 kcal mol^{-1} at pH 10, Figure 2a). At a higher solution pH of 20 (Figure 2b), formation of Re(CHO) is only slightly uphill (+2.2 kcal mol^{-1}), while conversion of Re(CHO) to $[Re(CHOH)]^+$ (step 2) is much more difficult (+12.8 kcal mol^{-1}).

Taken together, the first H^- (step 1) and H^+ (step 2) transfers are equivalent to a net addition of H_2 across the CO ligand. At 1 atm of H_2, $[Re(CHOH)]^+$ will always be 15.0 kcal mol^{-1} higher in energy than $[Re(CO)]^+$, regardless of the solution pH. In principal the thermodynamic barrier for H_2 addition can be eliminated by increasing the pressure of H_2. However, the large $\Delta G°_{H_2}$ value of 15.0 kcal mol^{-1} for $[Re(CO)]^+$ means that an experimentally insurmountable H_2 pressure of 1×10^{11} atm would be required for $[Re(CO)]^+$ and $[Re(CHOH)]^+$ to be isoenergetic. At an experimentally attainable H_2 pressure of 500 atm, $[Re(CHOH)]^+$ would still be 11.4 kcal mol^{-1} higher in free energy than $[Re(CO)]^+$. Selection of a solution pH of 20 at P_{H_2} = 500 atm would result in Re(CHO) being the lowest-energy species, and protonation of Re(CHO) to afford $[Re(CHOH)]^+$ would have an energetic penalty of 12.8 kcal mol^{-1} (Figure 2c).

The free energy landscapes also illustrate the necessity of using model complexes in order to measure thermodynamic properties related to reduction of $[CpRe(PPh_3)(NO)(CO)]^+$. For example, all of the open-shell species containing C−H and O−H bonds are high in energy, consistent with the irreversible electrochemistry due to favorable hydrogen atom transfer to a second equivalent of the same complex to generate two closed-shell species that are each 20−30 kcal mol^{-1} lower in energy. Similarly, at pH 10 (Figure 2a), $[CpRe(PPh_3)(NO)(CHOH)]^+$

dx.doi.org/10.1021/ja502316e | J. Am. Chem. Soc. 2014, 136, 8661−8668

and $CpRe(PPh_3)(NO)(CHO)$ are nearly isoenergetic and are interchangeable by proton transfer, however, hydride-transfer results in the formation of the equally energetic $CpRe(PPh_3)(NO)(CH_2OH)$ and the much lower in energy species $[CpRe(PPh_3)(NO)(CO)]^+$. The hydride-transfer reaction is favorable by 15 kcal mol^{-1}, which prevents the direct determination of the pK_a value unless the analogous methylated complex is used as a surrogate.

Tuning the Thermodynamic Properties. Since large values of $\Delta G^\circ_{H_2}$ for $[Re(CO)]^+$ represent a thermodynamic impediment for catalysis, it is desirable to control the magnitude of $\Delta G^\circ_{H_2}$. As seen in Figure 3a, DFT computations

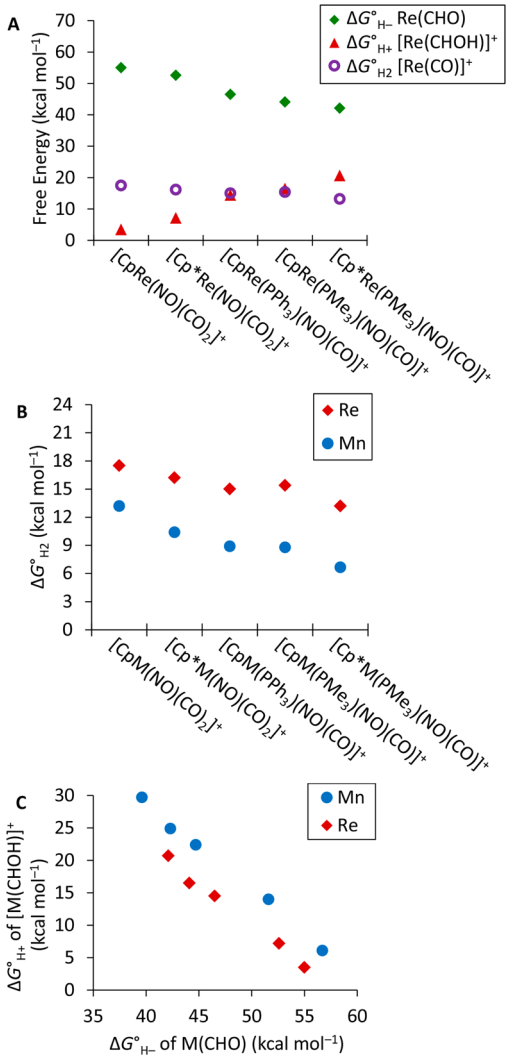

Figure 3. Plot of (A) $\Delta G^\circ_{H^-}$, $\Delta G^\circ_{H^+}$, and $\Delta G^\circ_{H_2}$ for varying $[Cp^XRe(L)(NO)(CO)]^+$ complexes, (B) $\Delta G^\circ_{H_2}$ for varying $[Cp^XM(L)(NO)(CO)]^+$ complexes, and (C) $\Delta G^\circ_{H^+}$ versus $\Delta G^\circ_{H^-}$ for varying $[Cp^XM(L)(NO)(CO)]^+$ complexes.

on a series of $[Cp^XRe(L)(NO)(CO)]^+$ complexes indicate that $\Delta G^\circ_{H_2}$ decreases by 4 kcal mol^{-1} upon progressing from $[CpRe(NO)(CO)_2]^+$ to $[Cp^*Re(PMe_3)(NO)(CO)]^+$, i.e., as the ancillary ligands become stronger σ-donors and weaker π-acceptors. The trend of decreasing $\Delta G^\circ_{H_2}$ parallels the decrease of $\Delta G^\circ_{H^-}$ values that were measured experimentally for the analogous series of $Cp^XRe(L)(NO)(CHO)$ complexes,[28,36] which means that $[Re(CO)]^+$ becomes a poorer H^- acceptor as it becomes a better H_2 acceptor. However, the decrease in $\Delta G^\circ_{H^-}$ of $Cp^XRe(L)(NO)(CHO)$ is accompanied by an increase in the basicity of the formyl ligand, indicated by the increase in free energy for proton dissociation from $[Cp^XRe(L)(NO)(CHOH)]^+$ ($\Delta G^\circ_{H^+}$ = 1.364 × pK_a, Figure 3a). The trends for $\Delta G^\circ_{H^-}$ and $\Delta G^\circ_{H^+}$ have an opposing effect on $\Delta G^\circ_{H_2}$, leading to the modest decrease in $\Delta G^\circ_{H_2}$ across the series of complexes.

Similar ancillary ligand effects are observed for the corresponding Mn complexes. However, $\Delta G^\circ_{H_2}$ of each $[Cp^XMn(L)(NO)(CO)]^+$ complex is 4–6 kcal mol^{-1} smaller than its Re congener (Figure 3b). Thus, by varying both the ancillary ligands and metal identity, $\Delta G^\circ_{H_2}$ can be reduced by approximately 11 kcal mol^{-1} across this series of complexes. For $[Cp^*Mn(PMe_3)(NO)(CO)]^+$, the complex with the lowest $\Delta G^\circ_{H_2}$ value (6.7 kcal mol^{-1}) in this series, $[Mn(CHOH)]^+$ would be only 3.0 kcal mol^{-1} higher in energy than $[Mn(CO)]^+$ at a pressure of H_2 of 500 atm. Therefore, the $\Delta G^\circ_{H_2}$ value of $[Cp^*Mn(PMe_3)(NO)(CO)]^+$ represents a significant improvement in the thermodynamics for reduction of the CO ligand compared to the Re analogues.

For the electrocatalytic cycle proposed in Scheme 1, M(CHO) is formed by intermolecular H^- transfer from $[HM(diphosphine)_2]^+$ (M = Ni, Pd, Pt). Therefore, the H^- acceptor ability of $[M(CO)]^+$ must be properly tuned to match the H^- donor ability of $[HM(diphosphine)_2]^+$. As described above, ancillary ligand variations that make H_2 addition more favorable also make the CO ligand a poorer H^- acceptor, which severely hinders the ability to tune the thermodynamics for catalytic CO reduction. In contrast, the $[Mn(CHOH)]^+$ complexes are less acidic than their $[Re(CHOH)]^+$ counterparts by 3–9 kcal mol^{-1}, while analogous Mn(CHO) and Re(CHO) complexes are comparable hydride donors (within 2.5 kcal mol^{-1}, Figure 3c). Thus, switching from Re to Mn allows the H_2 acceptor ability of the CO ligand to be changed independently of its H^- acceptor ability.

The rhenium and manganese complexes all possess a large free energy for H_2 addition to the CO ligand and thus are incapable of effectively catalyzing CO reduction. However, the significant decrease in free energy for H_2 addition upon shifting from Re to Mn suggests that carbonyl complexes of other metals may not have the same thermodynamic limitations. We are currently exploring whether additional periodic effects can be utilized to further improve the thermodynamics of $[M(CO)]^+$ reduction.

SUMMARY AND CONCLUSIONS

An extended thermochemical scheme was developed for reduction of $[CpRe(PPh_3)(NO)(CO)]^+$ to $CpRe(PPh_3)(NO)(CH_2OH)$ by using model complexes that do not undergo undesirable side reactions. Insights into chemical reactivity were obtained by converting the thermochemical data into free energy landscapes, in which the relative free energies of reaction intermediates can be illustrated under varying conditions of pH and P_{H_2}. For a reduction mechanism involving sequential H^- and H^+ transfers to the CO ligand, $[CpRe(PPh_3)(NO)(CHOH)]^+$ was found to be a high energy intermediate due to a large free energy requirement for the net addition of H_2 to $[CpRe(PPh_3)(NO)(CO)]^+$. DFT computations predict that $\Delta G^\circ_{H_2}$ can be tuned by ~11 kcal mol^{-1} by varying both the

dx.doi.org/10.1021/ja502316e | J. Am. Chem. Soc. 2014, 136, 8661–8668

ancillary ligands and metal in a series of $[Cp^XM(L)(NO)(CO)]^+$ complexes. Notably, switching from Re to Mn led to a significant improvement in the H_2 acceptor ability of the CO complexes without appreciable detriment to the H^- acceptor ability. Through this comparison of Re and Mn complexes, it is apparent that the choice of metal can provide substantial control over the relative energies of catalytic intermediates, thereby allowing tuning of critical factors such as the free energy for the addition of H_2.

EXPERIMENTAL SECTION

Methods and Materials. All manipulations were carried out under N_2 using standard vacuum line, Schlenk, and inert-atmosphere glovebox techniques. Acetonitrile (Alfa-Aesar, anhydrous, amine-free) was purified by sparging with N_2 and passage through neutral alumina using an Innovative Technology, Inc., Pure Solv solvent purification system. Acetonitrile-d_3 (Cambridge Isotope Laboratories) was vacuum-distilled from P_2O_5. Water was dispensed from a Millipore Milli-Q purifier and sparged with nitrogen. Tetrabutylammonium hexafluorophosphate (Fluka, ≥99%) was used as received. *o*-Toluidine (Fluka, ≥99.5%) was degassed via three consecutive freeze−pump−thaw cycles and dried over neutral alumina. *o*-Toluidinium tetrafluoroborate was prepared by reaction of o-toluidine with 1.5 equiv of $HBF_4{\cdot}Et_2O$ followed by recrystallization from CH_3CN/Et_2O. All Re complexes were synthesized according to literature procedures.[20,37,38,40,52]

Instrumentation. ^{1}H NMR spectra were recorded on a Varian NMR S spectrometer (500 MHz for ^{1}H) at 25 °C. All ^{1}H chemical shifts have been internally calibrated using the monoprotio impurity of the deuterated solvent. Calorimetry experiments were performed using a GE MicroCal iTC200. Voltammetry measurements were performed using a CH Instruments 620D potentiostat equipped with a standard three-electrode cell.

pK_a Determination. $[CpRe(PPh_3)(NO)(CMeOH)](OTf)$ (15 mM) was equilibrated with four different concentrations of *o*-toluidine (8−23 mM) in CD_3CN solution and monitored by ^{1}H NMR spectroscopy. Averaged resonances were observed due to rapid exchange between the protonated and deprotonated forms of each species, and the ratio of each species was determined from the weighted average of the chemical shifts. The equilibrium was also measured in the reverse direction using *o*-toluidinium tetrafluoroborate (11 mM) and three separate concentrations of $CpRe(PPh_3)(NO)(CMeO)$ (5−19 mM). The measured equilibrium constants and the known pK_a value of *o*-toluidinium (10.50)[39] were used to calculate a pK_a 10.6 ± 0.4 for $[CpRe(PPh_3)(NO)(CMeOH)](OTf)$, where the listed error is twice the standard deviation of the measurements.

Attempted Equilibrium H^- Transfer. $CpRe(PPh_3)(NO)(CH_2OMe)$ (10.9 mg, 0.019 mmol, 1.0 equiv) and $[Cp^*Re(CO)_2(NO)](BF_4)$ (7.2 mg, 0.015 mmol, 0.8 equiv) were combined in 0.7 mL CD_3CN, and the reaction conversion to $[CpRe(PPh_3)(NO)(CHOMe)]^+$ (0.5 equiv), $CpRe(PPh_3)(NO)(CH_3)$ (0.5 equiv), and $[Cp^*Re(CO)(NO)(COOMe)]$ (0.5 equiv) was monitored periodically by ^{1}H NMR spectroscopy. A reaction conversion of 80% was observed at 45 min, and a reaction conversion of 100% was observed at 2 h 15 min. The identity of each species was confirmed by comparison to the ^{1}H NMR chemical shifts recorded on independently prepared samples.

Calorimetry. Calorimetry measurements were recorded under inert atmosphere in a glovebox. Acetonitrile stock solutions of $CpRe(PPh_3)(NO)(CHO)$ (6.2 mM) and $[CpRe(PPh_3)(NO)(CHOMe)](OTf)$ (10.7 mM) were prepared, and the concentrations were determined by ^{1}H NMR spectroscopy using hexamethyldisiloxane as an integration standard. The reaction cell of the calorimeter was loaded by syringe with 230 μL of the $CpRe(PPh_3)(NO)(CHO)$ solution, the injection syringe was loaded with the $[CpRe(PPh_3)(NO)(CHOMe)](OTf)$ solution, and the reference cell was loaded with neat acetonitrile. Stirring was commenced at 1000 rpm, and the system was equilibrated at 25.0 °C. Upon equilibration, 15 injections of 1 μL $[CpRe(PPh_3)(NO)(CMeOH)](OTf)$ solution were added to the cell with a 4 min delay between injections. The first data point was discarded, and the average enthalpy per mol for the subsequent 14 injections was −11.3 ± 0.2 kcal mol^{-1}. This procedure was performed a total of 6 times using 3 independently prepared sets of stock solutions, resulting in an average enthalpy of −11.5 ± 2.6 kcal mol^{-1} (error listed at 2σ).

Electrochemistry. Cyclic voltammograms were recorded in a glovebox at ambient temperature, 23 ± 2 °C, using a 5 mL conical glass vial fitted with a polysilicone cap having openings sized to closely accept each electrode. The working electrode (1 mm PEEK-encased glassy carbon disc, ALS) was polished using diamond paste (Buehler, 0.25 μm) on a polishing pad wet with purified H_2O, then the electrode was rinsed with neat acetonitrile. A glassy carbon rod (Structure Probe, Inc.) was used as the counterelectrode, and a silver wire suspended in a solution of Bu_4NPF_6 (0.2 M) in acetonitrile and separated from the analyte solution by a Vycor frit (CH Instruments 112) was used as a pseudoreference electrode. Ferrocene or cobaltocenium hexafluorophosphate ($E_{1/2}$ = −1.33 V) was used as an internal standard, and all potentials are referenced to the ferrocenium/ferrocene couple at 0 V.

Computational Details. All calculations were carried out with the program Gaussian 09.[53] Structures were optimized without symmetry constraints using the B3P86[54,55] functional. The Stuttgart basis set with effective core potential (ECP)[56] was used for the Re and Mn atoms, whereas the 6-31G* basis set[57,58] was used for all other atoms with one additional *p* polarization function [$\xi(p)$ = 1.1] for the hydrogens located on the CHOH and CHO ligands. Each structure was confirmed by a frequency calculation at the same level of theory to be a real local minimum on the potential energy surface without imaginary frequency. For each species, the gas-phase free energy was calculated at 298 K in the harmonic approximation. Solvation free energies in acetonitrile were calculated by using the polarizable continuum model (C-PCM)[59,60] using Bondi[61] atomic radii. Several rotational isomers were considered for each complex containing a CHOH or CHO ligand, and the lowest-energy conformations were used in the thermodynamic calculations (see Supporting Information for details). This computational setup has been shown to accurately predict thermodynamic properties of $[HNi(diphosphine)_2]^{2+}$ complexes with a mean absolute error of <2 kcal mol^{-1}.[51]

ASSOCIATED CONTENT

Supporting Information

NMR spectra, cyclic voltammograms, tabulation of thermochemical cycles, description of computational conformational analysis, energies from DFT calculations, complete refs 7, 13, and 53, a text file of all computed molecule Cartesian coordinates in a format for convenient visualization, and an interactive spreadsheet for construction of free energy landscapes for $[CpRe(PPh_3)(NO)(CO)]^+$. This material is available free of charge via the Internet at http://pubs.acs.org.

AUTHOR INFORMATION

Corresponding Author

eric.wiedner@pnnl.gov

Notes

The authors declare no competing financial interest.

ACKNOWLEDGMENTS

This work was supported by the US Department of Energy, Office of Basic Energy Sciences, Division of Chemical Sciences, Geosciences & Biosciences. Computational resources were provided at the National Energy Research Scientific Computing Center (NERSC) at Lawrence Berkeley National Laboratory. Pacific Northwest National Laboratory (PNNL) is a multiprogram national laboratory operated for DOE by Battelle.

REFERENCES

(1) Costentin, C.; Robert, M.; Saveant, J.-M. *Chem. Soc. Rev.* **2013**, *42*, 2423−2436.
(2) Windle, C. D.; Perutz, R. N. *Coord. Chem. Rev.* **2012**, *256*, 2562−2570.
(3) Kondratenko, E. V.; Mul, G.; Baltrusaitis, J.; Larrazabal, G. O.; Perez-Ramirez, J. *Energy Environ. Sci.* **2013**, *6*, 3112−3135.
(4) DuBois, D. L. *Inorg. Chem.* **2014**, *53*, 3921−4268.
(5) Schneider, J.; Jia, H. F.; Muckerman, J. T.; Fujita, E. *Chem. Soc. Rev.* **2012**, *41*, 2036−2051.
(6) Oh, Y.; Hu, X. *Chem. Soc. Rev.* **2013**, *42*, 2253−2261.
(7) Appel, A. M.; et al. *Chem. Rev.* **2013**, *113*, 6621−6658.
(8) Savéant, J.-M. *Chem. Rev.* **2008**, *108*, 2348−2378.
(9) Benson, E. E.; Kubiak, C. P.; Sathrum, A. J.; Smieja, J. M. *Chem. Soc. Rev.* **2009**, *38*, 89−99.
(10) Bartholomew, C. H.; Farrauto, R. J. *Fundamentals of Industrial Catalytic Processes*, 2nd ed.; Wiley-VCH: Hoboken, NJ, 2006.
(11) Olah, G. A.; Goeppert, A.; Prakash, G. K. S. *Beyond Oil and Gas: the Methanol Economy*, Wiley-VCH: Weinheim, 2006.
(12) Khodakov, A. Y.; Chu, W.; Fongarland, P. *Chem. Rev.* **2007**, *107*, 1692−1744.
(13) Arakawa, H.; et al. *Chem. Rev.* **2001**, *101*, 953−996.
(14) Cook, T. R.; Dogutan, D. K.; Reece, S. Y.; Surendranath, Y.; Teets, T. S.; Nocera, D. G. *Chem. Rev.* **2010**, *110*, 6474−6502.
(15) Cutler, A. R.; Hanna, P. K.; Vites, J. C. *Chem. Rev.* **1988**, *88*, 1363−1403.
(16) West, N. M.; Miller, A. J. M.; Labinger, J. A.; Bercaw, J. E. *Coord. Chem. Rev.* **2011**, *255*, 881−898.
(17) Gladysz, J. A. *Adv. Organomet. Chem.* **1982**, *20*, 1−38.
(18) Torrent, M.; Solà, M.; Frenking, G. *Chem. Rev.* **2000**, *100*, 439−494.
(19) Marko, L. *Transition Met. Chem.* **1992**, *17*, 474−480.
(20) Tam, W.; Lin, G. Y.; Wong, W. K.; Kiel, W. A.; Wong, V. K.; Gladysz, J. A. *J. Am. Chem. Soc.* **1982**, *104*, 141−152.
(21) Gibson, D. H.; Owens, K.; Mandal, S. K.; Sattich, W. E.; Franco, J. O. *Organometallics* **1991**, *10*, 1203−1206.
(22) Lapinte, C.; Catheline, D.; Astruc, D. *Organometallics* **1988**, *7*, 1683−1691.
(23) Tanaka, K.; Ooyama, D. *Coord. Chem. Rev.* **2002**, *226*, 211−218.
(24) Berke, H.; Huttner, G.; Weiler, G.; Zsolnai, L. *J. Organomet. Chem.* **1981**, *219*, 353−362.
(25) Vaughn, G. D.; Gladysz, J. A. *Organometallics* **1984**, *3*, 1596−1598.
(26) Vaughn, G. D.; Gladysz, J. A. *J. Am. Chem. Soc.* **1986**, *108*, 1473−1480.
(27) Miedaner, A.; DuBois, D. L.; Curtis, C. J.; Haltiwanger, R. C. *Organometallics* **1993**, *12*, 299−303.
(28) Ellis, W. W.; Miedaner, A.; Curtis, C. J.; Gibson, D. H.; DuBois, D. L. *J. Am. Chem. Soc.* **2002**, *124*, 1926−1932.
(29) Elowe, P. R.; West, N. M.; Labinger, J. A.; Bercaw, J. E. *Organometallics* **2009**, *28*, 6218−6227.
(30) Teets, T. S.; Labinger, J. A.; Bercaw, J. E. *Organometallics* **2013**, *32*, 5530−5545.
(31) Imler, G. H.; Zdilla, M. J.; Wayland, B. B. *J. Am. Chem. Soc.* **2014**, *136*, 5856−5859.
(32) Fu, X.; Li, S.; Wayland, B. B. *Inorg. Chem.* **2006**, *45*, 9884−9889.
(33) Fu, X.; Wayland, B. B. *J. Am. Chem. Soc.* **2005**, *127*, 16460−16467.
(34) Wayland, B. B.; Van Voorhees, S. L.; Wilker, C. *Inorg. Chem.* **1986**, *25*, 4039−4042.
(35) Farnos, M. D.; Woods, B. A.; Wayland, B. B. *J. Am. Chem. Soc.* **1986**, *108*, 3659−3663.
(36) Ellis, W. W.; Ciancanelli, R.; Miller, S. M.; Raebiger, J. W.; Rakowski DuBois, M.; DuBois, D. L. *J. Am. Chem. Soc.* **2003**, *125*, 12230−12236.
(37) Sweet, J. R.; Graham, W. A. G. *J. Am. Chem. Soc.* **1982**, *104*, 2811−2815.
(38) Buhro, W. E.; Wong, A.; Merrifield, J. H.; Lin, G. Y.; Constable, A. C.; Gladysz, J. A. *Organometallics* **1983**, *2*, 1852−1859.
(39) Kaljurand, I.; Kutt, A.; Soovali, L.; Rodima, T.; Maemets, V.; Leito, I.; Koppel, I. A. *J. Org. Chem.* **2005**, *70*, 1019−1028.
(40) Tetrick, S. M.; Tham, F. S.; Cutler, A. R. *J. Am. Chem. Soc.* **1997**, *119*, 6193−6194.
(41) Hupp, J. T.; Weaver, M. J. *Inorg. Chem.* **1984**, *23*, 3639−3644.
(42) Nicholson, R. S.; Shain, I. *Anal. Chem.* **1964**, *36*, 706−723.
(43) Bard, A. J.; Faulkner, L. R. *Electrochemical Methods: Fundamentals and Applications*, 2nd ed.; John Wiley & Sons: Hoboken, NJ, 2001.
(44) Wayner, D. D. M.; Parker, V. D. *Acc. Chem. Res.* **1993**, *26*, 287−294.
(45) Parker, V. D.; Handoo, K. L.; Roness, F.; Tilset, M. *J. Am. Chem. Soc.* **1991**, *113*, 7493−7498.
(46) Tilset, M.; Parker, V. D. *J. Am. Chem. Soc.* **1989**, *111*, 6711−6717.
(47) Appel, A. M.; Lee, S. J.; Franz, J. A.; DuBois, D. L.; Rakowski DuBois, M. *J. Am. Chem. Soc.* **2009**, *131*, 5224−5232.
(48) Appel, A. M.; Lee, S. J.; Franz, J. A.; DuBois, D. L.; Rakowski DuBois, M.; Twamley, B. *Organometallics* **2009**, *28*, 749−754.
(49) Roberts, J. A. S.; Appel, A. M.; DuBois, D. L.; Bullock, R. M. *J. Am. Chem. Soc.* **2011**, *133*, 14604−14613.
(50) Ciancanelli, R.; Noll, B. C.; DuBois, D. L.; Rakowski DuBois, M. *J. Am. Chem. Soc.* **2002**, *124*, 2984−2992.
(51) Chen, S.; Rousseau, R.; Raugei, S.; Dupuis, M.; DuBois, D. L.; Bullock, R. M. *Organometallics* **2011**, *30*, 6108−6118.
(52) Agbossou, F.; O'Connor, E. J.; Garner, C. M.; Méndez, N. Q.; Fernández, J. M.; Patton, A. T.; Ramsden, J. A.; Gladysz, J. A.; O'Connor, J. M.; Tajima, T.; Gable, K. P. Cyclopentadienyl Rhenium Complexes. In *Inorganic Syntheses*; John Wiley & Sons, Inc.: Hoboken, NJ, 1992; pp 211−225.
(53) Frisch, M. J. et al. *Gaussian 09*; revision B.01; Gaussian, Inc.: Wallingford, CT, 2010.
(54) Becke, A. D. *J. Chem. Phys.* **1993**, *98*, 5648−5652.
(55) Perdew, J. P. *Phys. Rev. B* **1986**, *33*, 8822−8824.
(56) Andrae, D.; Haussermann, U.; Dolg, M.; Stoll, H.; Preuss, H. *Theor. Chem. Acc.* **1990**, *77*, 123−141.
(57) Francl, M. M.; Pietro, W. J.; Hehre, W. J.; Binkley, J. S.; Gordon, M. S.; Defrees, D. J.; Pople, J. A. *J. Chem. Phys.* **1982**, *77*, 3654−3665.
(58) Rassolov, V. A.; Ratner, M. A.; Pople, J. A.; Redfern, P. C.; Curtiss, L. A. *J. Comput. Chem.* **2001**, *22*, 976−984.
(59) Barone, V.; Cossi, M. *J. Phys. Chem. A* **1998**, *102*, 1995−2001.
(60) Cossi, M.; Rega, N.; Scalmani, G.; Barone, V. *J. Comput. Chem.* **2003**, *24*, 669−681.
(61) Bondi, A. *J. Phys. Chem.* **1964**, *68*, 441−451.